

Competing Lattice and Defect Dynamics Govern Terahertz-Induced Ferroelectricity in Quantum Paraelectric SrTiO₃

L. Cheng,¹ K. Hu,¹ S. Yang,¹ Yan Liang,² Jiandi Zhang,² and J. Qi^{1,*}

¹*State Key Laboratory of Electronic Thin Films and Integrated Devices,
University of Electronic Science and Technology of China, Chengdu 610054, China*

²*Beijing National Laboratory for Condensed Matter Physics,
Institute of Physics, Chinese Academy of Science, Beijing 100190, China*

arXiv:2512.01253v1 [cond-mat.mtrl-sci] 1 Dec 2025

Abstract

Intense terahertz (THz) pulses induce transient inversion-symmetry breaking in quantum paraelectric SrTiO₃, yet the underlying mechanism remains controversial. Using fields up to ~ 1.1 MV/cm, we reveal spatially inhomogeneous THz-field-induced second harmonic generation (TFISH) governed by competing lattice and defect dynamics. Short-lived coherent antiferrodistortive (AFD) modes suppress dipole correlations within ~ 5 ps, while heavily damped soft/AFD modes and a defect-induced low-frequency mode (~ 0.1 - 0.3 THz) jointly prevent long-range ferroelectric coherence in oxygen-vacancy-rich regions. Collective modes manifested by oscillatory TFISH components exhibit softening followed by hardening below a critical temperature $T^* \simeq 28$ K, confirming transient ferroelectric order where defects are sparse. These results reconcile conflicting interpretations, establish defect-mediated competition as a central regulator of light-induced ferroelectricity, and open routes to ultrafast control of quantum materials.

Quantum paraelectric oxides such as SrTiO₃ (STO) and KTaO₃ (KTO) possess incipient ferroelectric (FE) soft modes that soften dramatically with decreasing temperature, yet quantum fluctuations stabilize the centrosymmetric phase down to $T = 0$ [1, 2]. STO follows the Curie-Weiss law with an extrapolated $T_C \simeq 35$ K but the dielectric constant saturates below T_{QP} (~ 50 K) [3]. KTO displays analogous behavior with a much lower T_C ($\simeq 4$ K) [4]. Similarly, below T_{QP} , frequency of the soft mode nearly saturates [5, 6] and deviates from the decreasing trend, which means they do not transform into the FE state but quantum paraelectric (QPE) phase. In order to restore the FE phase, permanent ferroelectricity can be induced by ¹⁸O substitution [7, 8] or strain engineering [9], but these methods irreversibly alter the lattice.

Intense terahertz (THz) pulses offer a reversible route to drive transient symmetry breaking in quantum paraelectrics STO [10–13] and KTO [14–16]. THz-field-induced second harmonic generation (TFISH) signals reveal broken inversion symmetry, but their microscopic origin remains disputed: transient long-range FE order [10, 11], dipolar correlations among polar nanoregions (PNRs) [14, 15], or hot-phonon effects [16] have all been proposed. The unavoidable presence of defects (particularly oxygen vacancies) introduces low-energy collective modes and further complicates interpretation [17].

Here, we use THz fields up to ~ 1.1 MV/cm to excite STO single crystal at positions with markedly different oxygen-vacancy concentrations (characterized by Raman spectroscopy [18], see Supplemental Material). Time- and spatial-resolved TFISH uncovers a dynamical competition: coherent antiferrodistortive (AFD) modes transiently suppress dipolar correlations, while defect

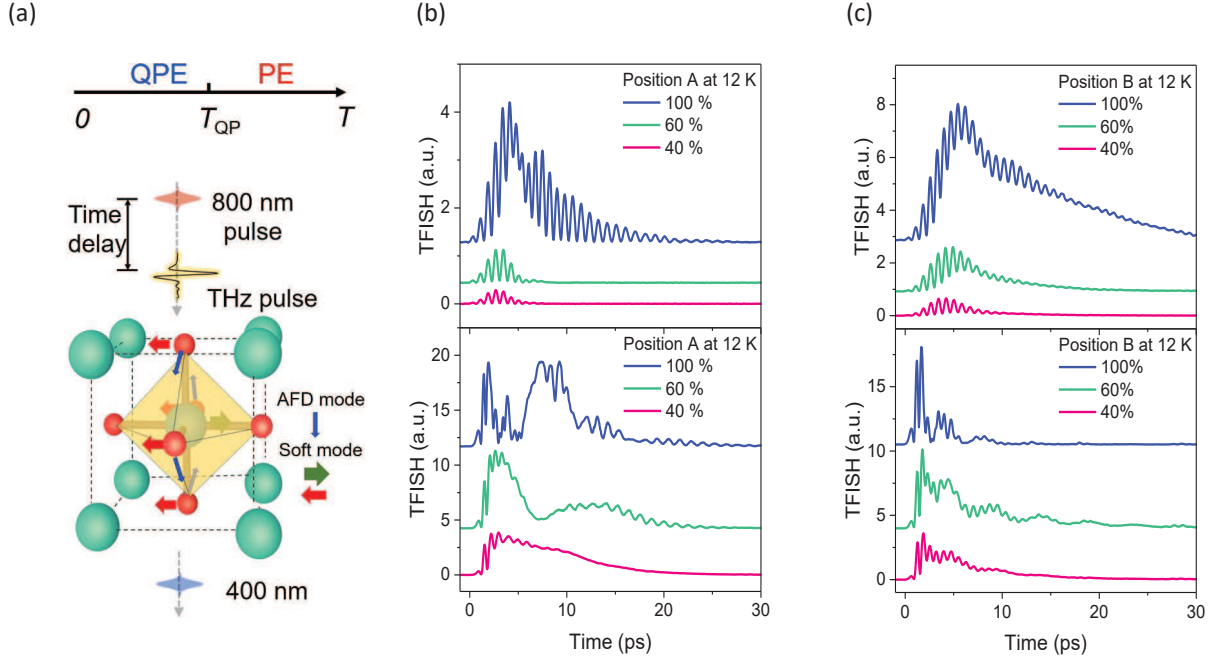


FIG. 1. (a) Schematic of time-resolved TFISH. Top: phase diagram of SrTiO₃ with T_{QP} separating quantum paraelectric (QPE) and paraelectric (PE) regimes. Atomic displacements of soft and AFD modes are sketched. (b-c) TFISH traces at positions A (low oxygen-vacancy density) and B (high oxygen-vacancy density) at 12 K under multi-cycle resonant (center frequency of ~ 0.65 THz and bandwidth of 0.25 THz) and single-cycle excitation for different field strengths (100%, 60%, 40% of peak fields $E_m^p \simeq 220$ kV/cm and $E_s^p \simeq 1.1$ MV/cm). Striking position dependence highlights the pivotal role of defects.

pinning and mode damping prevent FE coherence in vacancy-rich region. Only in clean regions do collective modes exhibit softening-to-hardening transitions below a critical temperature $T^* \simeq 28$ K, revealing light-induced long-range FE order deep within the quantum paraelectric regime.

Figure 1(a) illustrates the experimental configuration: a THz pump impulsively drives the lattice, and a delayed 800-nm probe detects transient SHG at 400 nm [19, 20]. Without THz excitation, no SHG is observed at any temperature in the sample. In the tetragonal phase below 110 K, both the soft mode and AFD mode exist [2, 5]. The former is infrared active and can be resonantly excited via the THz pulse [10, 11, 13–16]. Here, both single-cycle and multi-cycle THz pulses are chosen. Given the pivotal role of defects (oxygen vacancies) in this type of study [15, 17], measurements are performed on STO sample with intentionally varied defect densities, prepared to elucidate their impact on the THz-induced phase transition.

Figures 1(b,c) show representative TFISH traces at 12 K. At sufficiently strong THz electric

fields, both oscillatory and non-oscillatory components are prominent, with dramatic differences between low-defect (position A) and high-defect (position B) regions. The oscillatory component originates from coherently THz-driven collective excitations and the nonlinear coupling among different modes [10, 12, 14–16]. The non-oscillatory component reflects quasi-static inversion symmetry breaking due to various debated candidates [10, 11, 13–16, 21].

The TFISH response exhibits strong nonlinearity with THz field strength. Under multi-cycle excitation, oscillations persist up to ~ 30 ps at peak field. With single-cycle pulses, signals at intermediate fields (i.e. 40% of $E_s^p \simeq 1.1$ MV/cm) are similar at both positions, showing decaying non-oscillatory backgrounds superimposed with complex oscillations. At high fields approaching to E_s^p , however, behavior diverges dramatically: within the first ~ 5 ps the non-oscillatory component is strongly suppressed at both positions, but re-emerges prominently thereafter only at position A, remaining nearly absent at position B. This reveals competing, time- and defect-dependent mechanisms governing the stabilization of transient inversion symmetry breaking.

Multi-cycle resonant excitation provides a cleaner probe of temperature-dependent dynamics (Fig. 2). At position A, the non-oscillatory TFISH amplitude and lifetime rise rapidly with decreasing temperature, peak at $T^* \simeq 28$ K, and then slowly decrease (Figs. 2(a,c)) – behaviour incompatible with continuous increasing as T reduces via mechanism such as PNR correlations or hot-phonon heating alone [15, 16]. Therefore, additional competing effect should appear below T^* . Fourier spectra of the oscillatory component (Fig. 2(e)) reveal multiple coherent modes. Below ~ 35 K, dominant weight appears near twice the soft-mode frequency ($2\nu_s \sim 1.3$ THz), which softens on cooling and abruptly hardens below T^* . This hardening mirrors the growth of a FE order parameter observed in ^{18}O -substituted STO [7, 8] and constitutes direct evidence of a transient FE phase emerging in the pristine QPE regime. Under off-resonant multi-cycle excitation (center frequency of ~ 0.4 THz, away from the soft-mode resonance), amplitude of the TFISH signal is nearly independent on the excitation frequency (Supplemental Material) and sharply contradicts with the highly frequency-dependence predicted by the hot-phonon effect [16], suggesting insignificant role of this effect.

By contrast, position B – rich in oxygen vacancies – shows no such anomaly (Figs. 2(d,f)). Amplitude and lifetime of the non-oscillatory component grow monotonically with decreasing temperature, and all modes soften continuously without reversal. Specifically, all the collective modes are strongly damped at low temperatures in this region, as demonstrated by the time-domain oscillations after the THz pulse duration in Fig. 2(b). Such damped situation dramatically lowers

the efficiency of coherent THz driving of both soft and AFD modes, preventing both the nonlinear displacement needed for ferroelectricity [10, 11, 13] and the transient lattice distortion that suppresses dipolar correlations [22, 23] in vacancy-sparse regions.

Raman characterization averages oxygen-vacancy density over our $\sim 80 \mu\text{m}$ probe area (a limited spatial resolution of $\sim 60 \mu\text{m}$), so microscopic inhomogeneity persists even within nominally uniform positions A and B. Consequently, the probed region can exhibit behavior akin to spatial phase coexistence: domains dominated by short-range PNR correlations coexist with domains supporting THz-induced long-range FE order. Both contributions add to the second-order susceptibility, $\chi^{(2)} = \chi_{\text{FE}}^{(2)} + \chi_{\text{PNRs}}^{(2)}$, and, however, compete in the TFISH signal. In sparsely defective position A, their comparable magnitudes yield the observed anomaly – non-oscillatory amplitude and lifetime increase with cooling initially attributed to dipolar PNR correlations, peak at $T^* \simeq 28 \text{ K}$ as FE order emerges, then decrease due to their competition. In oxygen-vacancy-rich position B, dipolar PNR correlations overwhelmingly dominate, producing monotonic temperature dependence and no detectable FE transition.

Single-cycle pulses at intense fields, e.g. $\sim 1.1 \text{ MV/cm}$, dramatically alter the TFISH signals in the time domain and indicate potential dynamical competing effects. In specific, within the first $\sim 5 \text{ ps}$, non-oscillatory component is almost completely quenched at both positions (Figs. 3(a,b)). The Fourier spectra exhibit abundant frequencies with spectral weight extending up to $\sim 2.7 \text{ THz}$ (Figs. 3(c,d)), which is not observed in case of the multi-cycle excitation. Previous investigation reveals large spectral weight of AFD mode and its coupled modes with soft phonon in STO appearing between 0.6 THz and 2.6 THz via the nonlinear phonon coupling [10]. Since the Ti-O-Ti bond-angle distortions via AFD modes cause weakening of dipole–dipole interactions and lead to transiently suppress both FE condensation and dipolar PNR correlations [22, 23] (the initial quench of non-oscillatory component can be intuitively understood). Considering both soft mode (Q_s) and AFD mode (Q_a), we can use the coupled oscillators to simulate such suppression in the time domain, evidenced by $Q_s(t)$ developing gradually from an unstable state approaching to a steady nonzero value and the effective potential of the soft mode evolving between single-well and double-well types due to influence of $Q_a(t)$ [3, 24–26] (see details in Supplemental Material).

After $\sim 5 \text{ ps}$ the AFD coherence decays (Figs. 3(a,e,f)), releasing the transient suppression of dipolar correlations and allowing symmetry-breaking signals to recover. In defect-sparse regions (position A), a delayed non-oscillatory component re-emerges and exhibits a distinct two-step temperature dependence below $\sim 28 \text{ K}$ (T^*): a slow rise followed by a much steeper escalation below

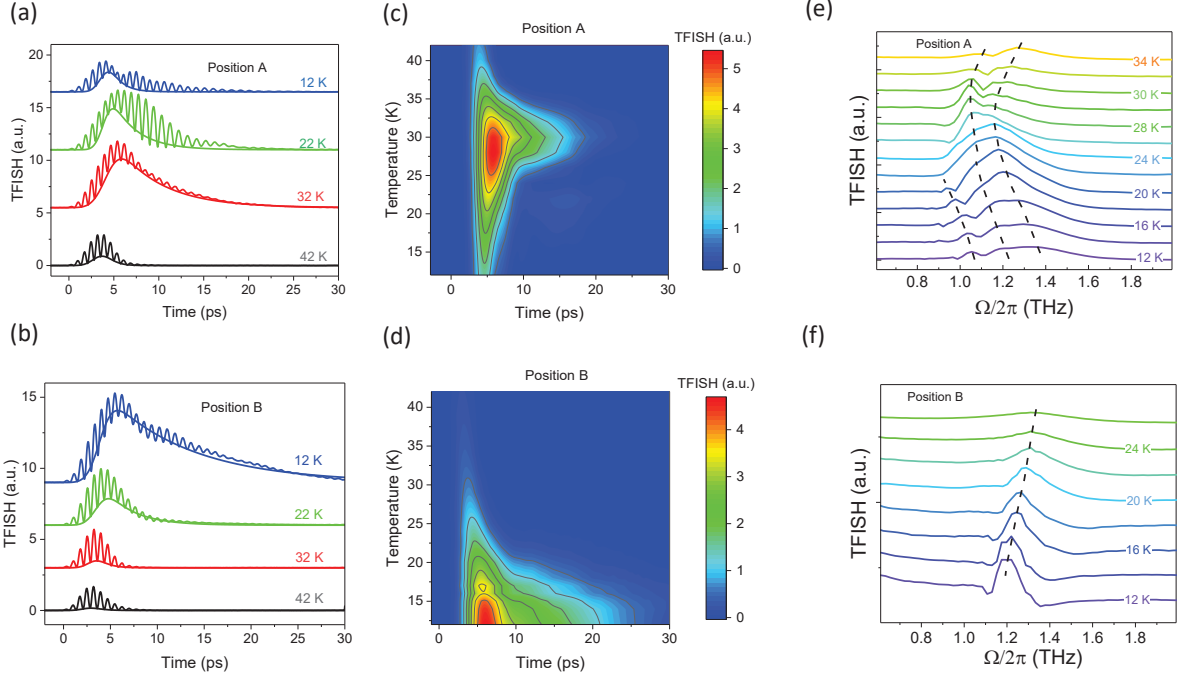


FIG. 2. Temperature evolution of TFISH under resonant multi-cycle excitation ($E_m^p \simeq 220$ kV/cm) with a pulse duration of $\tau_{\text{THz}}^m (\sim 5$ ps). (a),(b) Time-domain traces at positions A and B for several typical temperatures. The solid lines indicate the non-oscillatory components approximated using the exponential decay fitting [15]. (c),(d) The non-oscillatory component after τ_{THz}^m as a function of temperature in the time domain. (e),(f) Fourier spectra of the oscillatory components extracted after τ_{THz}^m . Position A exhibits clear maxima near $T^* \simeq 28$ K for the non-oscillatory component, and subsequent softening-to-hardening of collective modes, while position B shows monotonic behaviour characteristic of defect-dominated dynamics. Dashed lines are guide for eyes.

~ 20 K (Fig. 3(f)), accompanied by collective modes showing anomalies near T^* (Figs. 3(c,e))—confirming the onset of transient FE order. However, The T -dependent amplitude reflects subtle competition between the nascent FE phase and persisting dipolar PNR correlations.

The FE contribution remains relatively weaker than under resonant multi-cycle pumping because it is re-established only after the decay of AFD coherence, which has a lifetime larger than the THz pulse duration. Consequently, short-range PNR correlations, which strengthen rapidly on cooling together with the potential hot-phonon effect, grow faster than the nascent FE order. This prevents the sharp peak and subsequent decline observed under multi-cycle excitation (Fig. 2(c)) and leads to PNR dominance at low temperatures.

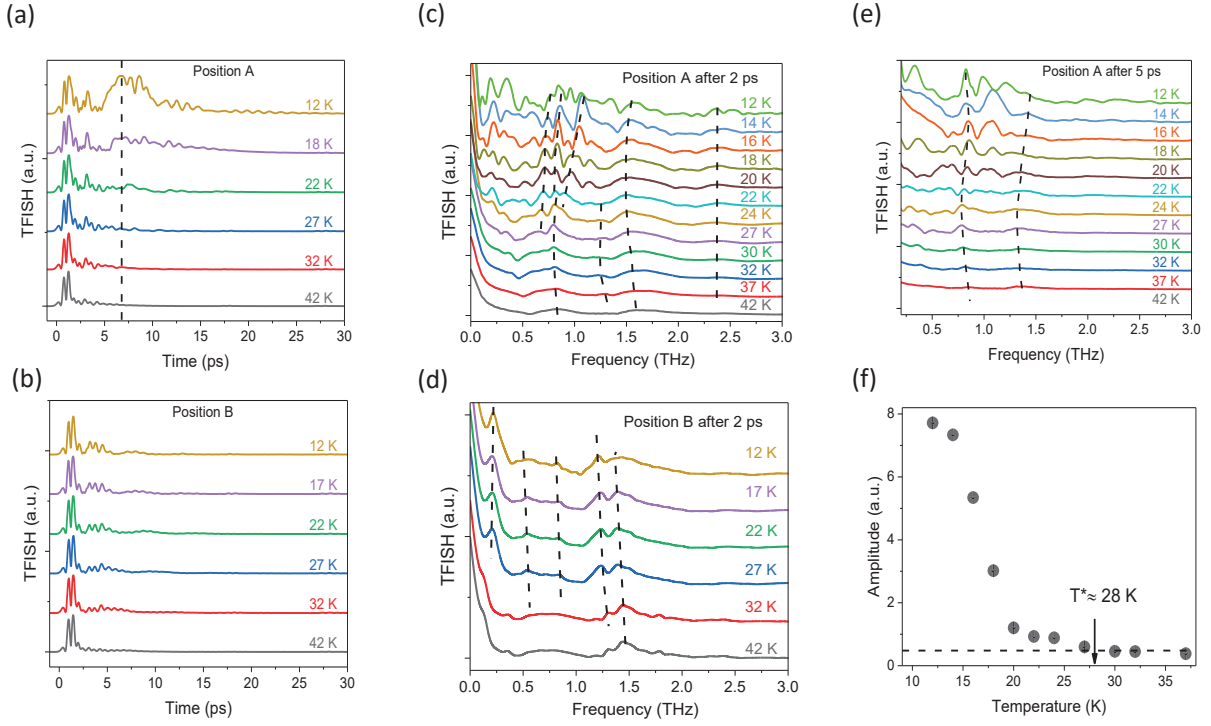


FIG. 3. Single-cycle excitation at $E_s^P \sim 1.1$ MV/cm with a THz pulse duration of $\tau_{\text{THz}}^s (\sim 2$ ps). (a-b) Time-domain TFISH traces at several typical temperatures in positions A and B. (c),(e) Fourier spectra after τ_{THz}^s (left) and after 5 ps (right) in position A, respectively. (d) Fourier spectra after τ_{THz}^s in position B. (f) The amplitude of non-oscillatory component at time indicated by the dashed line in (a) as a function of temperature. Dashed lines are guide for eyes.

At position B, however, the delayed recovery is essentially absent. This is consistent with observation that the THz-triggered coherent oscillations are strongly damped and survive only within ~ 5 ps (Fig. 3(b)). Their frequencies undergo monotonic changes as a function of temperature (Fig. 3(d)), suggesting no phase transition. Notably, a low-frequency mode (~ 0.1 - 0.3 THz) emerges at low temperatures and can persist for ~ 30 ps, as evidenced by the distinct slow oscillations in time-domain (Fig. 1(c)). This low-energy mode hardens either with THz field increasing (Fig. 1(c)) or upon cooling (Fig. 3(d)). Its characteristics—including frequency value, temperature-dependent stiffening and confinement to oxygen-vacancy-rich regions—identify it as a defect-induced collective mode associated with PNRs [17]. Our findings suggest that strongly and coherently excitation of this mode will prevent the establishment of global FE coherence and inhibit the dipolar PNR correlations.

Although intense broadband single-cycle pulses inevitably generate a large non-equilibrium

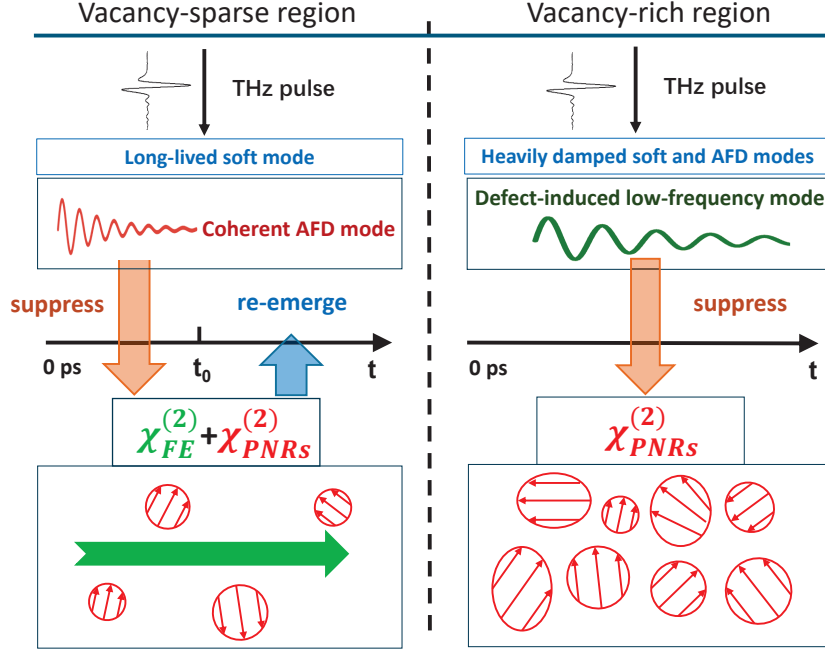


FIG. 4. Competing THz-driven pathways in quantum paraelectric SrTiO₃. **Left (oxygen-vacancy-sparse region, position A)**: Exciting coherent AFD rotations transiently suppress dipolar correlations within t_0 (orange arrow), e.g. $t_0 \simeq 5$ ps for single-cycle pulse with $E_s^p = 1.1$ MV/cm. After decay, transient ferroelectricity driven by coherent soft-mode and THz-induced correlations of PNRs re-emerge (blue arrow). Non-oscillatory TFISH signals include competing contributions determined by the second-order susceptibility tensors: $\chi_{FE}^{(2)}$ and $\chi_{PNRs}^{(2)}$. **Left (oxygen-vacancy-rich region, position B)**: Soft and AFD modes are heavily damped; a persistent defect-induced low-frequency mode (~ 0.1 - 0.3 THz, dark-green oscillation) dominates and frustrates global coherence, preventing transient ferroelectricity and suppressing dipolar correlations of local polar clusters (PNRs). Non-oscillatory TFISH signals are dominantly contributed by $\chi_{PNRs}^{(2)}$.

phonon population in both positions, the hot-phonon scenario [16] should play minor role: it predicts the TFISH signal undergoing a quadratic increase with the THz electric-field, which in stark contrast to the universal early-time quenching and spatial-dependent recovery in the TFISH data at high fields. This is consistent with the inference from results of multi-cycle excitation.

Our experiments reveal several competing THz-driven processes in STO (schematic in Fig. 4): (i) Short-lived coherent AFD modes ($\lesssim 5$ ps) universally suppress inversion symmetry breaking immediately after intense single-cycle THz excitation. (ii) In oxygen-vacancy-rich regions, heavily damped soft/AFD modes reduce driving efficiency, while a persistent defect-pinned mode (~ 0.1 - 0.3 THz) frustrates both long-range FE order and dipolar correlations of PNRs. (iii) In

oxygen-vacancy-sparse regions, collective modes exhibit softening-to-hardening below $T^* \simeq 28$ K, confirming true THz-induced ferroelectricity, which coexists and competes with the dipolar correlations of PNRs. These results reconcile divergent literature interpretations. The THz-induced transient FE phase [10, 11, 13] emerges only when defect density is low and AFD suppression decays. PNR-dominated [14, 15] or hot-phonon [16] scenario can describe defective or lower-field regimes but fail under clean, high-field conditions.

In summary, intense THz excitation initiates a dynamical hierarchy in which lattice distortions, mode damping, and defect pinning compete on picosecond timescales. By mapping this competition at the single-crystal level, we demonstrate that defects are active regulators—not passive scatterers—of light-induced quantum criticality, paving the way for reversible, ultrafast engineering of emergent order in perovskite oxides and beyond.

This work was supported by the National Key R&D Program of China (Grant Nos. 2022YFA1403000 and 2024YFA1408502), the National Natural Science Foundation of China (Grants No. 12434003, No. 92365102, No. 62027807, and No. 12474107), the CAS project for Yong Scientists in Basic Research (Grant No. YSBR-030) and the Guangdong Basic and Applied Basic Research Foundation (Grant No. 2024A1515011600).

* jbqi@uestc.edu.cn

- [1] R. A. Cowley, Lattice dynamics and phase transitions of strontium titanate, *Phys. Rev.* **134**, A981 (1964).
- [2] J. F. Scott, Soft-mode spectroscopy: Experimental studies of structural phase transitions, *Rev. Mod. Phys.* **46**, 83 (1974).
- [3] K. A. Müller and H. Burkard, SrTiO_3 : An intrinsic quantum paraelectric below 4 K, *Phys. Rev. B* **19**, 3593 (1979).
- [4] H. Fujishita, S. Kitazawa, M. Saito, R. Ishisaka, H. Okamoto, and T. Yamaguchi, Quantum paraelectric states in SrTiO_3 and KTaO_3 : Barrett model, vendik model, and quantum criticality, *Journal of the Physical Society of Japan* **85**, 074703 (2016), <https://doi.org/10.7566/JPSJ.85.074703>.
- [5] H. Vogt, Refined treatment of the model of linearly coupled anharmonic oscillators and its application to the temperature dependence of the zone-center soft-mode frequencies of KTaO_3 and SrTiO_3 , *Physical Review B* **51**, 8046 (1995).

- [6] Y. Yamada and G. Shirane, Neutron scattering and nature of the soft optical phonon in SrTiO_3 , *Journal of the Physical Society of Japan* **26**, 396 (1969), <https://doi.org/10.1143/JPSJ.26.396>.
- [7] M. Takesada, M. Itoh, and T. Yagi, Perfect softening of the ferroelectric mode in the isotope-exchanged strontium titanate of $\text{SrTi}^{18}\text{O}_3$ studied by light scattering, *Phys. Rev. Lett.* **96**, 227602 (2006).
- [8] M. Itoh, R. Wang, Y. Inaguma, T. Yamaguchi, Y.-J. Shan, and T. Nakamura, Ferroelectricity induced by oxygen isotope exchange in strontium titanate perovskite, *Phys. Rev. Lett.* **82**, 3540 (1999).
- [9] J. H. Haeni, P. Irvin, W. Chang, R. Uecker, P. Reiche, Y. L. Li, S. Choudhury, W. Tian, M. E. Hawley, B. Craigo, A. K. Tagantsev, X. Q. Pan, S. K. Streiffer, L. Q. Chen, S. W. Kirchoefer, J. Levy, and D. G. Schlom, Room-temperature ferroelectricity in strained SrTiO_3 , *Nature* **430**, 758 (2004).
- [10] X. Li, T. Qiu, J. Zhang, E. Baldini, J. Lu, A. M. Rappe, and K. A. Nelson, Terahertz field-induced ferroelectricity in quantum paraelectric SrTiO_3 , *Science* **364**, 1079 (2019), <https://www.science.org/doi/pdf/10.1126/science.aaw4913>.
- [11] T. F. Nova, A. S. Disa, M. Fechner, and A. Cavalleri, Metastable ferroelectricity in optically strained SrTiO_3 , *Science* **364**, 1075–1079 (2019).
- [12] M. Basini, M. Pancaldi, B. Wehinger, M. Udina, V. Unikandanunni, T. Tadano, M. C. Hoffmann, A. V. Balatsky, and S. Bonetti, Terahertz electric-field-driven dynamical multiferroicity in SrTiO_3 , *Nature* **628**, 534 (2024).
- [13] D. Shin, S. Latini, C. Schäfer, S. A. Sato, E. Baldini, U. De Giovannini, H. Hübener, and A. Rubio, Simulating terahertz field-induced ferroelectricity in quantum paraelectric SrTiO_3 , *Phys. Rev. Lett.* **129**, 167401 (2022).
- [14] X. Li, P. Peng, H. Dammak, G. Geneste, A. Akbarzadeh, S. Prosandeev, L. Bellaiche, and D. Talbayev, Terahertz pulse induced second harmonic generation and kerr effect in the quantum paraelectric KTO_3 , *Phys. Rev. B* **107**, 064306 (2023).
- [15] B. Cheng, P. L. Kramer, Z.-X. Shen, and M. C. Hoffmann, Terahertz-driven local dipolar correlation in a quantum paraelectric, *Phys. Rev. Lett.* **130**, 126902 (2023).
- [16] F. Yang, X. J. Li, D. Talbayev, and L. Q. Chen, Terahertz-induced second-harmonic generation in quantum paraelectrics: Hot-phonon effect, *Phys. Rev. Lett.* **135**, 056901 (2025).
- [17] G. Orenstein, V. Krapivin, Y. Huang, Z. Zhang, G. de la Peña Muñoz, R. A. Duncan, Q. Nguyen, J. Stanton, S. Teitelbaum, H. Yavas, T. Sato, M. C. Hoffmann, P. Kramer, J. Zhang, A. Cavalleri, R. Comin, M. P. M. Dean, A. S. Disa, M. Först, S. L. Johnson, M. Mitrano, A. M. Rappe, D. A. Reis, D. Zhu, K. A. Nelson, and M. Trigo, Observation of polarization density waves in SrTiO_3 ,

- Nature Physics **21**, 1026 (2025), arXiv:2403.17203 [cond-mat.mtrl-sci].
- [18] D. Chapron, F. Cordero, and M. D. Fontana, Characterization of oxygen vacancies in SrTiO_3 by means of anelastic and raman spectroscopy, *J. Appl. Phys.* **126**, 154101 (2019).
- [19] Y. Gao, X. Y. Zeng, X. B. Wang, Y. G. Shi, L. Cheng, and J. Qi, Terahertz manipulation of nonlinear optical response in topological material PtBi_2 , *Opt. Lett.* **49**, 3862 (2024).
- [20] K. Hu, Y. Qin, L. Cheng, Y. Shi, and J. Qi, Giant nonlinear optical response in topological semimetal molybdenum phosphide, *Chinese Physics Letters* **40**, 114202 (2023).
- [21] W. Li, H. Kim, X. Wang, J. Luo, S. Latini, D. Shin, J.-M. Liu, J.-F. Li, A. Rubio, C.-W. Nan, and Q. Li, A hidden quantum paraelectric phase in SrTiO_3 induced by terahertz field (2024), arXiv:2412.20887 [cond-mat.mtrl-sci].
- [22] W. Zhong and D. Vanderbilt, Competing structural instabilities in cubic perovskites, *Phys. Rev. Lett.* **74**, 2587 (1995).
- [23] I. A. Kornev, L. Bellaiche, P.-E. Janolin, B. Dkhil, and E. Suard, Phase diagram of $\text{Pb}(\text{Zr}, \text{Ti})\text{O}_3$ solid solutions from first principles, *Phys. Rev. Lett.* **97**, 157601 (2006).
- [24] J. G. Bednorz and K. A. Müller, $\text{Sr}_{1-x}\text{Ca}_x\text{TiO}_3$: An XY quantum ferroelectric with transition to randomness, *Phys. Rev. Lett.* **52**, 2289 (1984).
- [25] M. Fechner, M. Först, G. Orenstein, V. Krapivin, A. S. Disa, M. Buzzi, A. von Hoegen, G. de la Pena, Q. L. Nguyen, R. Mankowsky, M. Sander, H. Lemke, Y. Deng, M. Trigo, and A. Cavalleri, Quenched lattice fluctuations in optically driven SrTiO_3 , *Nature Materials* **23**, 363 (2024), arXiv:2301.08703 [cond-mat.mtrl-sci].
- [26] T. Gu, T. Scarbrough, Y. Yang, J. Íñiguez, L. Bellaiche, and H. J. Xiang, Cooperative couplings between octahedral rotations and ferroelectricity in perovskites and related materials, *Phys. Rev. Lett.* **120**, 197602 (2018).